Available online at www.sciencedirect.com
SCIENCE DIRECT®
Journal of Sound and Vibration 284 (2005) 75–102
JOURNAL OF SOUND AND VIBRATION
www.elsevier.com/locate/jsvi

Nonlinear random responses of a structure parametrically coupled with liquid sloshing in a cylindrical tank

Takashi Ikeda[a,*], R.A. Ibrahim[b]

[a]*Department of Electronic and Control Systems Engineering, Shimane University, 1060 Nishikawatsu, Matsue, 690-8504 Japan*
[b]*Department of Mechanical Engineering, Wayne State University, Detroit, MI 48202, USA*

Received 13 May 2003; received in revised form 6 January 2004; accepted 6 June 2004
Available online 15 December 2004

Abstract

The nonlinear random interaction of an elastic structure with liquid sloshing dynamics in a cylindrical tank is investigated in the neighborhood of 2:1 internal resonance. Such internal resonance takes place when the natural frequency of the elastic structure is close to twice the natural frequency of the anti-symmetric sloshing mode (1,1). The excitation is generated from the response of a linear shaping filter subjected to a Gaussian white noise. The analytical model involves three sloshing modes (1,1), (0,1) and (2,1). The system response statistics and stability boundaries are numerically estimated using Monte Carlo simulation. The influence of the excitation center frequency, its bandwidth, and the liquid level on the system responses is studied. It is found that there is an irregular energy exchange between the structure and the liquid free surface motion when the center frequency is close to the structure natural frequency. Depending on the excitation power spectral density, the liquid free surface experiences zero motion, uncertain motion (intermittency), partially developed motion, and fully developed random motion. The structure response probability density function is almost Gaussian, while the liquid elevation deviates from normality. The unstable region, where the liquid motion occurs, becomes wider as the excitation intensity increases or as the bandwidth decreases. As the liquid depth or the structure spring stiffness decreases, the region of nonlinear interaction shrinks and is associated with a shift of the peak of the structure mean square response toward the left side of the frequency axis.

*Corresponding author. Fax: +81 852 32 8909.
E-mail addresses: tikeda@riko.shimane-u.ac.jp (T. Ikeda), ibrahim@eng.wayne.edu (R.A. Ibrahim).

0022-460X/$ - see front matter © 2004 Elsevier Ltd. All rights reserved.
doi:10.1016/j.jsv.2004.06.049

Nomenclature

c	damping coefficient of structure
F_l	vertical fluid force
$F(t)$	narrow-band random excitation
$\mathbf{g}$	acceleration of gravity
h	liquid depth
k	structure stiffness
M	total mass of structure and liquid ($= m + m_l$)
m	mass of structure
m_l	mass of liquid
P	fluid hydrodynamic pressure
R	tank radius
(r, θ, z)	circular cylindrical coordinate system (see Fig. 1)
S_0	power spectrum density of white noise
t	time
$W(t)$	Gaussian white noise
(x, y, z)	rectangular coordinate system (see Fig. 1)
Z_0	displacement of structure
β	angular position of nodal diameter
γ	bandwidth of a narrow-band random excitation
ζ_{mn}	damping ratios of (m, n) sloshing mode
η	displacement of liquid surface
μ_1	$= m/M$
μ_2	$= m_l R/(\pi M h)$
ρ	fluid density
Φ	velocity potential function
Ω	center frequency of a narrow-band random excitation
ω_s	structure natural frequency
ω_{mn}	natural frequency of the (m, n) sloshing mode

1. Introduction

The problem of liquid sloshing interaction with structural dynamics may fall into one of the following categories:

1. Interaction of liquid sloshing dynamics with the container elastic modes. Two limiting cases may occur where interaction disappears [1]. The first case deals with the excitation of liquid surface modes where significant elastic modes of the container are not participating. In this case, the analysis of the liquid in a rigid container will provide a satisfactory description of the overall behavior. The second case deals with the excitation of the container elastic modes where significant liquid motion does not occur. In this case, the presence of the liquid will contribute to the distributed mass to the tank walls, and the analysis can be carried out without considering any interaction with the liquid sloshing dynamics. Between these two limiting cases, one should consider the nonlinear interaction between liquid sloshing and structure mode in breathing and bending deformations.
2. Interaction of liquid sloshing dynamics with the supporting elastic structure. This type of interaction takes place between the free liquid surface motion and the supported elastic structure dynamics based on the assumption that the liquid container is rigid.
3. Liquid interaction with immersed elastic structures [2,3].

The first two categories have recently been reviewed by Ibrahim et al. [4]. The present work is related to the second category. Under base motion of liquid water towers, the fluid container

experiences motion in a certain trajectory governed by the excitation and the liquid response. The free liquid surface motion results in hydrodynamic forces that are fed back to the supporting structure. The dynamics of elevated water towers under seismic excitation was examined by Ifrim and Bratu [5], Sonobe and Nishikawa [6], van Erp [7], and Shepherd [8]. The nonlinear interaction in elevated water towers subjected to vertical sinusoidal ground motion was examined in the neighborhood of internal resonance by Ibrahim and Barr [9,10], Ibrahim [11], and Ibrahim and Li [12]. In these studies, the free liquid surface sloshing modes and the elastic support structure were coupled through inertia nonlinearity, which results in internal resonance conditions among the interacting modes (i.e., $\sum_{j=1}^{n} k_j\omega_j = 0$, where k_j are integers and ω_j are the natural frequencies of the coupled modes). This type of coupling is referred to as autoparametric interaction, and occurs when an externally excited mode can act as a parametric excitation to other modes. The problem of internal resonances in nonlinearly coupled oscillators is of interest in connection with redistribution of energy among the various natural modes. This energy sharing is usually brought about by resonant interactions among the natural modes of the system. The coupling among these modes plays a crucial role in such interactions. In a straightforward perturbation theory, internal resonances lead to the problem of small divisors (secular terms).

Under the principal internal resonance condition (i.e., when one of the normal mode frequencies is twice another mode frequency), the system possesses a steady-state response [9]. Ibrahim and Barr [10] found that under the summed or difference internal resonance conditions (i.e., one of the normal mode frequencies equals the sum or difference of another two mode frequencies) the system does not achieve a constant steady-state response.

Nonstationary responses of cases including violent system motion, which can lead to collapse of the system, were reported in the neighborhood of multiple internal resonances [11]. The multiple internal resonances may occur when two or more sloshing modes are interacting with the vertical and horizontal motions of the structure. In the neighborhood of the summed internal resonance and one-to-one internal resonance, the structure and free liquid surface simultaneously oscillate with a continuous increase in their amplitude. This growth could lead to structural failure if the shaker excitation is not stopped. In the presence of one-to-two and one-to-one internal resonance conditions, experimental observations showed a steady-state response over a frequency range defined by the regions of instability. The regions of instability were indicated by the occurrence of collapse in response amplitudes. Another type of instability, manifested by a jump in amplitudes, was caused by a weak energy flow between the fluid modes and structure modes for a few cycles. Within a short period of time, the system achieves a steady-state response.

Ibrahim and Li [12] studied liquid–structure interaction under horizontal periodic motion. Ikeda and Nakagawa [13] and Ikeda et al. [14] considered the nonlinear interaction of liquid sloshing in rectangular and cylindrical tanks with an elastic structure whose motion is orthogonal to the tank vertical walls. They showed that the frequency response curves experience change from soft to hard response characteristics as the water depth decreases. Under vertical sinusoidal excitation of an elastic structure carrying a rigid rectangular tank, Ikeda [15] and Ikeda and Murakami [16,17] determined the response of the coupled system when the structure natural frequency is about twice the liquid sloshing frequency. As the excitation frequency approached the structure natural frequency the free liquid surface was excited through the autoparametric resonance and energy was transferred from the structure to the free liquid surface. An asymptotic expansion of the wave height and velocity potential of the liquid coupled with structural dynamics

was developed by Limarchenko and Yasinsky [18] and Lukovskii and Timokha [19] for simplified models of spacecraft.

In the absence of internal resonance, Haroun and Elliathy [20,21] and Haroun et al. [22] combined a finite element model of a tower with a mechanical model of an elevated vessel. They included the hydrodynamic forces due to liquid sloshing and its interaction with the motion of the supporting tower. They found that the fundamental mode of sloshing combined with the lateral translation and the global rotation at the top of the supporting tower, yield maximum values for the shearing force and overturning moment on the tower. The flexibility of the tank wall would definitely increase these maximum forces, though such an effect can be neglected in small capacity tanks. Kareem and Sun [23] studied the stochastic response of structures with liquid tanks in the absence of internal resonance.

Soundararajan and Ibrahim [24] examined more realistic cases such as simultaneous random horizontal and vertical ground excitations in the presence of a 1:3 internal resonance. They used a Gaussian and non-Gaussian closure schemes to determine the system response statistics. They found that both Gaussian and non-Gaussian solutions deviate appreciably from the linear solution as the system approaches internal resonance but they converge when the system is detuned away from the exact internal resonance. The autoparametric interaction was identified by an irregular energy exchange between the two modes.

The concept of using sloshing hydrodynamic forces to control structure vibration has been recognized long time ago. It is known that shallow liquid levels in a container experience traveling sloshing waves. On the other hand, deeper liquid levels cause a standing sloshing wave in the fundamental mode. For large wave amplitudes, there is a critical depth, above which the liquid waves possess soft nonlinear spring characteristics and below that level, the nonlinearity is of the hard type. Furthermore, standing waves are associated with poor energy dissipation (see, e.g., Ref. [25]). The effectiveness of tuned liquid dampers (TLD) has been studied analytically, numerically, and experimentally. Most of the analytical studies did not follow the coupled differential equations of the liquid interaction with the support main structure. In some few cases, the coupling was considered numerically [26].

This paper deals with an elastic structure carrying a cylindrical tank partially filled with liquid where the structure is vertically subjected to a narrow-band random excitation. The modal equations are derived taking into account the liquid nonlinear inertia forces. Nonlinear coupling between liquid modes and structure modes results in 2:1 internal resonance, i.e., when the natural frequencies of the structure and the first anti-symmetric sloshing mode are commensurable. The modal equations are numerically solved using Monte Carlo simulation, and the system response statistics are estimated.

2. Theoretical analysis

2.1. Equations of motion

Fig. 1 shows a rigid circular cylindrical tank supported on an elastic structure represented by a mass m, spring stiffness k, and dashpot with damping coefficient c. The liquid tank has a radius R,

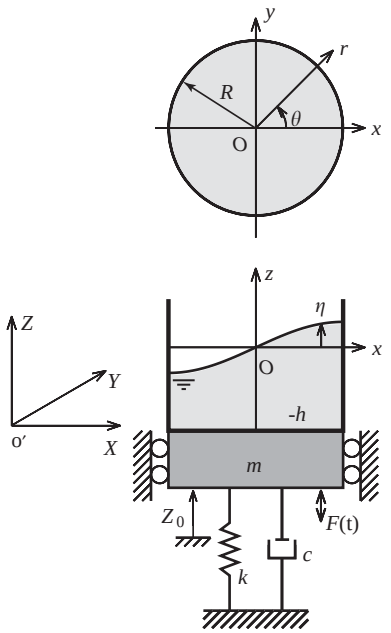

Fig. 1. The model for theoretical analysis.

and is partially filled with liquid to a depth h. A moving rectangular coordinate frame (x, y, z) and a circular cylindrical coordinate (r, θ, z), are fixed to the liquid undisturbed free surface. The xy-plane coincides with the equilibrium position of the liquid surface. The vertical displacement of the mass m, measured from its equilibrium position when the tank is partially filled is Z_0. The vertical displacement of the liquid surface is $\eta(r, \theta, t)$ measured from the undisturbed free surface. In terms of the velocity potential function $\Phi(r, \theta, z, t)$, the liquid motion inside the tank is governed by the continuity equation (Laplace's equation)

$$\frac{\partial^2 \Phi}{\partial r^2} + \frac{1}{r}\frac{\partial \Phi}{\partial r} + \frac{1}{r^2}\frac{\partial^2 \Phi}{\partial \theta^2} + \frac{\partial^2 \Phi}{\partial z^2} = 0. \tag{1}$$

The hydrodynamic pressure $P(r, \theta, z, t)$ is determined from Bernoulli's equation [9,27] (also see Appendix A)

$$\frac{\partial \Phi}{\partial t} + \frac{1}{2}\left\{\left(\frac{\partial \Phi}{\partial r}\right)^2 + \frac{1}{r^2}\left(\frac{\partial \Phi}{\partial \theta}\right)^2 + \left(\frac{\partial \Phi}{\partial z}\right)^2\right\} + gz + \frac{P}{\rho} = -\ddot{Z}_0 z, \tag{2}$$

where ρ is the fluid density, g is the acceleration of gravity, and a dot denotes differentiation with respect to time t.

The equation of motion of the structure subjected to vertical random excitation, $F(t)$, is

$$m\ddot{Z}_0 + c\dot{Z}_0 + kZ_0 = F_l + F(t) + m_l g, \tag{3}$$

where F_l is the fluid hydrodynamic force acting in the z-direction on the bottom of the tank, and m_l is the liquid mass. The fluid force F_l is given by integrating the fluid pressure at the bottom of the tank as follows:

$$F_l = -\int_0^{2\pi}\int_0^R rP(r,\theta,z,t)|_{z=-h}\,\mathrm{d}r\,\mathrm{d}\theta, \tag{4}$$

where $P(r,\theta,z,t)$ is determined from Eq. (2).

The random excitation $F(t)$ is assumed to be generated from the following linear shaping filter:

$$\frac{\mathrm{d}^2F}{\mathrm{d}t^2} + \gamma_0\frac{\mathrm{d}F}{\mathrm{d}t} + \Omega_0^2F = \Omega_0 W(t), \tag{5}$$

where γ_0 is the filter bandwidth, Ω_0 is the filter center frequency, $W(t)$ is a zero-mean Gaussian white noise possessing constant power spectral density D.

The following parameters are introduced:

$$\begin{aligned}
&z_0 = Z_0/R, \quad \bar{\eta} = \eta/R, \quad \bar{r} = r/R, \quad \bar{z} = z/R, \quad \bar{h} = h/R, \quad \mu_1 = m/M, \quad \mu_2 = m_l/(\pi M\bar{h}),\\
&\phi = \Phi/(R^2\omega_{11}), \quad \bar{k} = k/(M\omega_{11}^2), \quad \zeta = c/(M\omega_{11}), \quad f = F/(MR\omega_{11}^2), \quad w(\tau) = W(t)/(MR\omega_{11}^3),\\
&f_l = F_l/(MR\omega_{11}^2), \quad p = P/(\rho R^2\omega_{11}^2), \quad \tau = \omega_{11}t, \quad \xi_{mn} = \lambda_{mn}R, \quad \Omega = \Omega_0/\omega_{11}, \quad \gamma = \gamma_0/\omega_{11},\\
&M = m + m_l, \quad \omega_{11} = \sqrt{g\lambda_{11}\tanh(\lambda_{11}h)}, \quad \psi_{11} = \xi_{11}\tanh(\xi_{11}h/R), \quad \bar{\omega}_s = \sqrt{k/M}/\omega_{11},
\end{aligned} \tag{6}$$

where λ_{mn} is the nth positive root of the derivative of Bessel function $\mathrm{d}/\mathrm{d}r\{\mathrm{J}_m(\lambda r)\}|_{r=R} = 0$. The subscript (m,n) refers to m nodal lines and the nth-order to a nodal concentric circle. In terms of the new parameters (6), Eqs. (1)–(3), and (5) are

$$\frac{\partial^2\phi}{\partial\bar{r}^2} + \frac{1}{\bar{r}}\frac{\partial\phi}{\partial\bar{r}} + \frac{1}{\bar{r}^2}\frac{\partial^2\phi}{\partial\theta^2} + \frac{\partial^2\phi}{\partial\bar{z}^2} = 0, \tag{7}$$

$$\frac{\partial\phi}{\partial\tau} + \frac{1}{2}\left\{\left(\frac{\partial\phi}{\partial\bar{r}}\right)^2 + \frac{1}{\bar{r}^2}\left(\frac{\partial\phi}{\partial\theta}\right)^2 + \left(\frac{\partial\phi}{\partial\bar{z}}\right)^2\right\} + \frac{1}{\psi_{11}}\bar{z} + p = -\frac{\mathrm{d}^2z_0}{\mathrm{d}\tau^2}\bar{z}, \tag{8}$$

$$\mu_1\frac{\mathrm{d}^2z_0}{\mathrm{d}\tau^2} + \zeta\frac{\mathrm{d}z_0}{\mathrm{d}\tau} + \bar{k}z_0 = f_l + f(\tau) + \frac{\pi\mu_2\bar{h}}{\psi_{11}}, \tag{9}$$

$$\frac{\mathrm{d}^2f}{\mathrm{d}\tau^2} + \gamma\frac{\mathrm{d}f}{\mathrm{d}\tau} + \Omega^2f = \Omega w(\tau), \tag{10}$$

where

$$f_l = -\mu_2\int_0^{2\pi}\int_0^1 \bar{r}p(\bar{r},\theta,\bar{z},\tau)|_{\bar{z}=-\bar{h}}\,\mathrm{d}\bar{r}\,\mathrm{d}\theta \tag{11}$$

and $w(\tau)$ is a zero-mean stationary Gaussian white noise process with variance σ_w^2 and constant power spectral density intensity S_0.

The boundary conditions at the tank walls and bottom are

$$\left.\frac{\partial\phi}{\partial\bar{r}}\right|_{\bar{r}=1}=0 \quad \text{and} \quad \left.\frac{\partial\phi}{\partial\bar{z}}\right|_{\bar{z}=-\bar{h}}=0. \tag{12a,b}$$

The kinematic boundary condition requires that the velocity of the liquid surface in the vertical direction is equal to the vertical velocity of the fluid particle on the liquid surface [9,27],

$$\frac{\partial\bar{\eta}}{\partial\tau}=\frac{\partial\phi}{\partial\bar{z}}-\frac{\partial\phi}{\partial\bar{r}}\frac{\partial\bar{\eta}}{\partial\bar{r}}-\frac{1}{\bar{r}^2}\frac{\partial\phi}{\partial\theta}\frac{\partial\bar{\eta}}{\partial\theta} \quad (\text{at } \bar{z}=\bar{\eta}). \tag{13}$$

Since the pressure $p=0$ at the free surface $\bar{z}=\bar{\eta}$, the dynamic boundary condition is

$$\frac{\partial\phi}{\partial\tau}+\frac{1}{2}\left\{\left(\frac{\partial\phi}{\partial\bar{r}}\right)^2+\frac{1}{\bar{r}^2}\left(\frac{\partial\phi}{\partial\theta}\right)^2+\left(\frac{\partial\phi}{\partial\bar{z}}\right)^2\right\}+\frac{1}{\psi_{11}}\bar{z}=-\frac{\mathrm{d}^2z_0}{\mathrm{d}\tau^2}\bar{z} \quad \text{at } \bar{z}=\bar{\eta}. \tag{14}$$

Eq. (7) together with the boundary conditions (12)–(14) describe the fluid field equations, which are coupled with the structure equation of motion (9) and its filter equation (10).

2.2. Modal equations

The solution of Laplace's equation (7) that satisfies the boundary conditions (12) may be written in the form

$$\phi(\bar{r},\theta,\bar{z},\tau)=a_c(\tau)+\sum_{m=0}^{\infty}\sum_{n=1}^{\infty}\{a_{mn}(\tau)\cos m\theta+b_{mn}(\tau)\sin m\theta\}\mathrm{J}_m(\xi_{mn}\bar{r})\frac{\cosh\{\xi_{mn}(\bar{z}+\bar{h})\}}{\cosh(\xi_{mn}\bar{h})}. \tag{15}$$

The free surface elevation may also be written in the form

$$\bar{\eta}(\bar{r},\theta,\tau)=\sum_{m=0}^{\infty}\sum_{n=1}^{\infty}\{c_{mn}(\tau)\cos m\theta+d_{mn}(\tau)\sin m\theta\}\mathrm{J}_m(\xi_{mn}\bar{r}), \tag{16}$$

where a_c, a_{mn}, b_{mn}, c_{mn} and d_{mn} are the generalized coordinates. The term $a_c(\tau)$, in Eq. (15), is very important because it is associated with the fluid force, which will be determined in the nonlinear analysis in the next section. Since the position of the liquid surface at rest is taken at the origin (i.e., at $\bar{z}=0$), the constant term may not be necessary in Eq. (16).

In the present analysis we consider the interaction of the three sloshing modes (0, 1), (1, 1) and (2, 1) with the structure dynamics. Mode (1, 1) is the first anti-symmetric sloshing and has two different modal amplitudes c_{11} and d_{11} whose nodal diameters are perpendicular to each other. In the nonlinear analysis, these modes are coupled.

Introducing a small parameter ε, and defining the following orders of the amplitudes and the damping coefficient ζ:

$$a_{11},b_{11},c_{11},d_{11},z_0;\ \zeta\approx O(\varepsilon^{1/3}), \tag{17a}$$

$$a_c,a_{01},c_{01},a_{21},b_{21},c_{21},d_{21}\approx O(\varepsilon^{2/3}), \tag{17b}$$

$$a_{31},b_{31},c_{31},d_{31}\approx O(\varepsilon^{3/3}). \tag{17c}$$

The orders of all other amplitudes, which are not shown in relations (17), are assumed to be smaller than $O(\varepsilon)$. The procedure begins by considering $\bar{\eta}$ to be small, and expanding Eqs. (13) and (14) about $\bar{\eta}=0$ after substituting Eqs. (15) and (16). By expanding the result into a Fourier–Bessel series in terms of $\mathrm{J}_0(\xi_{01}\bar{r})$, $\mathrm{J}_m(\xi_{m1}\bar{r})\cos m\theta$ and $\mathrm{J}_m(\xi_{m1}\bar{r})\sin m\theta$ $(m=1,2)$, and equating the constant terms and the coefficients of $\mathrm{J}_0(\xi_{01}\bar{r})$, $\mathrm{J}_m(\xi_{m1}\bar{r})\cos m\theta$ and $\mathrm{J}_m(\xi_{m1}\bar{r})\sin m\theta$ on the both sides of these equations, gives the modal equations as follows:

The equation of motion of the structure is

$$Q_1\ddot{z}_0+\zeta\dot{z}_0+\bar{k}z_0+Q_2\dot{a}_c+G_1(a_{11},b_{11})=f(\tau). \tag{18a}$$

Sloshing modal equations of the first anti-symmetric mode are

$$\dot{a}_{11}+\left(\frac{1}{\psi_{11}}+\ddot{z}_0\right)c_{11}+G_2(\dot{a}_{i1},\dot{b}_{j1},a_{i1},b_{j1},c_{i1},d_{j1})=0, \tag{18b}$$

$$\dot{b}_{11}+\left(\frac{1}{\psi_{11}}+\ddot{z}_0\right)d_{11}+G_3(\dot{a}_{i1},\dot{b}_{j1},a_{i1},b_{j1},c_{i1},d_{j1})=0, \tag{18c}$$

$$\dot{c}_{11}-\psi_{11}a_{11}+G_4(a_{i1},b_{j1},c_{i1},d_{j1})=0, \tag{18d}$$

$$\dot{d}_{11}-\psi_{11}b_{11}+G_5(a_{i1},b_{j1},c_{i1},d_{j1})=0, \tag{18e}$$

$$\dot{a}_c+G_6(\dot{a}_{11},\dot{b}_{11},\dot{z}_0,a_{11},b_{11},c_{11},d_{11})=0. \tag{18f}$$

Sloshing modal equations of the first symmetric mode are

$$\dot{a}_{01}+\left(\frac{1}{\psi_{11}}+\ddot{z}_0\right)c_{01}+G_7(\dot{a}_{11},\dot{b}_{11},a_{11},b_{11},c_{11},d_{11})=0, \tag{18g}$$

$$\dot{c}_{01}-\psi_{01}a_{01}+G_8(a_{11},b_{11},c_{11},d_{11})=0, \tag{18h}$$

Sloshing modal equations of the second anti-symmetric mode are

$$\dot{a}_{21}+\left(\frac{1}{\psi_{11}}+\ddot{z}_0\right)c_{21}+G_9(\dot{a}_{11},\dot{b}_{11},a_{11},b_{11},c_{11},d_{11})=0, \tag{18i}$$

$$\dot{b}_{21}+\left(\frac{1}{\psi_{11}}+\ddot{z}_0\right)d_{21}+G_{10}(\dot{a}_{11},\dot{b}_{11},a_{11},b_{11},c_{11},d_{11})=0, \tag{18j}$$

$$\dot{c}_{21}-\psi_{21}a_{21}+G_{11}(a_{11},b_{11},c_{11},d_{11})=0, \tag{18k}$$

$$\dot{d}_{21}-\psi_{21}b_{21}+G_{12}(a_{11},b_{11},c_{11},d_{11})=0. \tag{18l}$$

where a dot denotes differentiation with respect to the nondimensional time parameter τ, $\psi_{m1}=\xi_{m1}\tanh(\xi_{m1}\bar{h})(m=0,1,2)$, $Q_1=\mu_1+\pi\mu_2\bar{h}$, and $Q_2=-\pi\mu_2$. $G_k(k=1,2,\ldots,12)$ represent the nonlinear terms, which consist of variables shown in their parentheses (see Appendix B). Eq. (18a) is obtained from the structure equation of motion (9). Eliminating a_c from Eqs. (18a) and (18f), gives

$$Q_1\ddot{z}_0+\zeta\dot{z}_0+\bar{k}z_0+G_{13}(\dot{a}_{11},\dot{b}_{11},a_{11},b_{11},c_{11},d_{11})=f(\tau), \tag{19}$$

where G_{13} is given in the appendix. Eliminating the variables $a_{11}, b_{11}, a_{01}, a_{21}$ and b_{21} from Eqs. (18) and (19) and considering the modal ordering assumption (17), gives as follows:

The structure equation of motion is

$$Q_1\ddot{z}_0 + \zeta\dot{z}_0 + \bar{k}z_0 + H_1(\ddot{z}_0, \dot{c}_{11}, \dot{d}_{11}, c_{11}, d_{11}) = f(\tau). \tag{20a}$$

Equations of motion of first anti-symmetric sloshing mode are

$$\ddot{c}_{11} + 2\zeta_{11}\dot{c}_{11} + (1 + \psi_{11}\ddot{z}_0)c_{11} + H_2(\dot{c}_{i1}, \dot{d}_{j1}, c_{i1}, d_{j1}) = 0, \tag{20b}$$

$$\ddot{d}_{11} + 2\zeta_{11}\dot{d}_{11} + (1 + \psi_{11}\ddot{z}_0)d_{11} + H_3(\dot{c}_{i1}, \dot{d}_{j1}, c_{i1}, d_{j1}) = 0. \tag{20c}$$

Equation of motion of first symmetric sloshing mode is

$$\ddot{c}_{01} + 2\zeta_{01}\omega_{01}\dot{c}_{01} + \omega_{01}^2(1 + \psi_{11}\ddot{z}_0)c_{01} + H_4(\ddot{z}_0, \dot{c}_{11}, \dot{d}_{11}, c_{11}, d_{11}) = 0. \tag{20d}$$

Equations of motion of second anti-symmetric sloshing mode are

$$\ddot{c}_{21} + 2\zeta_{21}\omega_{21}\dot{c}_{21} + \omega_{21}^2(1 + \psi_{11}\ddot{z}_0)c_{21} + H_5(\ddot{z}_0, \dot{c}_{11}, \dot{d}_{11}, c_{11}, d_{11}) = 0, \tag{20e}$$

$$\ddot{d}_{21} + 2\zeta_{21}\omega_{21}\dot{d}_{21} + \omega_{21}^2(1 + \psi_{11}\ddot{z}_0)d_{21} + H_6(\ddot{z}_0, \dot{c}_{11}, \dot{d}_{11}, c_{11}, d_{11}) = 0, \tag{20f}$$

where $\omega_{mn}^2 = \psi_{mn}/\psi_{11}$, and H_l $(l = 1\text{–}6)$ represent the nonlinear terms, which are listed in the appendix. It should be noted that viscous damping terms are added in Eqs. (20b)–(20f) in order to account for energy dissipation. ζ_{mn} is the damping ratio corresponding to sloshing mode (m, n). Eq. (20) involve quadratic and cubic inertia nonlinear coupling terms that give rise to the occurrence of internal resonance. From the nonlinear coupling terms in Eq. (20), it is not difficult to show that principal internal resonance can take place if the natural frequency of the structure $\bar{\omega}_s$ is close to twice the natural frequency of the first anti-symmetric sloshing mode.

2.3. Random excitation of the uncoupled system

This section considers the mean square response of the structure with the liquid as a frozen block. Such analysis is valuable in verifying the accuracy of Monte Carlo simulation and will be used to normalize the response of the coupled system. In this case, we consider the equation of motion

$$Q_1\ddot{z}_0 + \zeta\dot{z}_0 + \bar{k}z_0 = f(\tau), \tag{21}$$

where $f(\tau)$ is defined by Eq. (10). The autocorrelation function $R_{z_0}(\tau')$ of $z_0(\tau)$ is

$$R_{z_0}(\tau') = \int_{-\infty}^{\infty} |H(\mathrm{j}\omega)|^2 S_w(\omega) \mathrm{e}^{\mathrm{j}\omega\tau'}\, \mathrm{d}\omega, \tag{22}$$

where $H(\mathrm{j}\omega)$ is the frequency response function of $z_0(\tau)$ to $w(\tau)$ in a complex form, which can be obtained from the transfer function

$$H(s) = \frac{\Omega}{s^2 + \gamma s + \Omega^2} \cdot \frac{1}{Q_1 s^2 + \zeta s + \bar{k}}. \tag{23}$$

$S_w(\omega) = S_0(=\text{constant})$ is the power spectral density of the white noise. Substituting $\tau' = 0$ into Eq. (22), gives the mean square response $E[z_0^2]$

$$E[z_0^2] = R_{z_0}(0) = S_0 \int_{-\infty}^{\infty} |H(\mathrm{j}\omega)|^2 \,\mathrm{d}\omega$$
$$= \frac{\pi S_0\{(\zeta+\gamma Q_1)(Q_1\Omega^2+\zeta\gamma+\bar{k}) - Q_1(\gamma\bar{k}+\zeta\Omega^2)\}}{\bar{k}\{(\zeta+\gamma Q_1)(Q_1\Omega^2+\zeta\gamma+\bar{k})(\gamma k+\zeta\Omega^2) - \bar{k}\Omega^2(\zeta+\gamma Q_1)^2 - Q_1(\gamma\bar{k}+\zeta\Omega^2)^2\}}. \quad (24)$$

This solution is mainly used for verifying the Monte Carlo simulation. The white noise $w(\tau)$ is generated from a random number series with zero mean value and variance $\sigma_w^2 = 2\pi S_0/\Delta\tau$ by using a FORTRAN subroutine based on the Box and Muller method [28]. In the simulation, the power spectral density $S_w(\omega)$ is defined by

$$S_w(\omega) = \begin{cases} S_0 & (-\omega_N \leqslant \omega \leqslant \omega_N), \\ 0 & (-\infty < \omega < -\omega_N, \omega_N < \omega < \infty), \end{cases}$$

where ω_N is the Nyquist frequency, which is given by $\omega_N = 2\pi/(2\Delta\tau) = \pi/\Delta\tau$, with $\Delta\tau = 0.25$. Fig. 2 shows time history records of the Gaussian white nose $w(\tau)$, the narrow-band random force $f(\tau)$ and the displacement $z_0(\tau)$ of the structure using the Runge–Kutta–Gill method. Fig. 2 is obtained for fluid depth ratio $\bar{h} = 1.2$, structure mass ratio $\mu_1 = 0.87$, liquid mass ratio $\mu_2 = 0.034$, structure stiffness parameter $\bar{k} = 4.0$, structure damping parameter $\zeta = 0.03$, excitation spectral density $S_0 = 2.0 \times 10^{-7}$, filter bandwidth $\gamma = 0.1$ and filter center frequency ratio $\Omega = 2.0$. The mean square response of the structure was estimated using Monte Carlo simulations using 100 different sets of random number series. The analytical and numerical estimates of $E[z_0^2]$ were found in good agreement.

3. Numerical results

3.1. Random excitation of the coupled system

The nonlinear modal interaction of the liquid free surface motion and structure dynamics is considered using Monte Carlo simulation. The numerical simulation of Eq. (20) is carried out when the natural frequency ω_s of the structure system is close to twice the natural frequency of the sloshing mode (1,1), i.e., $\omega_s(\equiv \sqrt{k/M}) \approx 2\omega_{11}$. Fig. 3 shows a sample of time history records for $w(\tau)$, $f(\tau)$, z_0, $\bar{\eta}$, c_{11}, d_{11} and β, for the same values of parameters used in Fig. 2, and damping ratios $\zeta_{01} = \zeta_{11} = \zeta_{21} = 0.01$. The liquid elevation $\bar{\eta}(\bar{r},\theta)$ is estimated with reference to the position $(\bar{r},\theta) = (1,0)$. The initial values in integrating Eq. (20) are all 0.01. The displacement z_0 exhibits a narrow-band random process, while the time histories of c_{11} and d_{11} reflect irregular rotational motion of the nodal diameter. The rotation of the nodal diameter is measured by the angle β as defined in Fig. 4. This angle is estimated by considering the (1,1) sloshing mode and expressing the liquid elevation as follows:

$$\bar{\eta}(\bar{r},\theta) = (c_{11}\cos\theta + d_{11}\sin\theta)\mathrm{J}_1(\xi_{11}\bar{r}) = A\cos(\theta-\beta)\mathrm{J}_1(\xi_{11}\bar{r}), \quad (25)$$

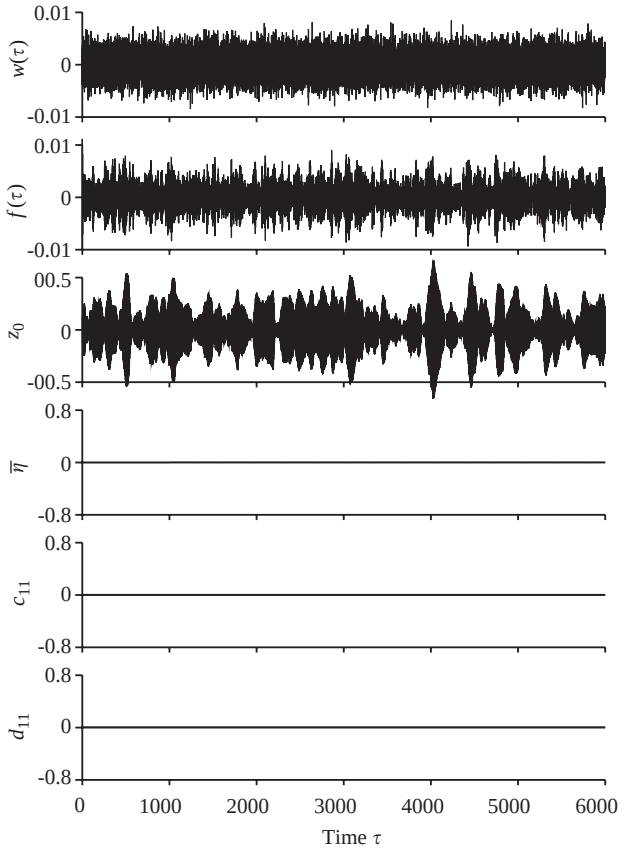

Fig. 2. Time histories in an uncoupled system (where the liquid is frozen) when $\bar{h} = 1.2$, $\mu_1 = 0.87$, $\mu_2 = 0.034$, $\bar{k} = 4.0$, $\zeta = 0.03$, $S_0 = 2.0 \times 10^{-7}$, $\gamma = 0.1$ and $\Omega = 2.0$.

where $A = \sqrt{c_{11}^2 + d_{11}^2}$ and $\beta = \tan^{-1}(d_{11}/c_{11})$. The numerical simulation reveals that the angle β is irregular as shown by the discretized points in Fig. 3.

Figs. 5(a)–(c) show three sets of time history records whose time axes are enlarged for the same parameters of Fig. 3. Each figure also includes the corresponding trajectories on the (c_{11}, d_{11})-plane for three time intervals (a) $1375 \leqslant \tau \leqslant 1500$, (b) $4500 \leqslant \tau \leqslant 4625$ and (c) $5000 \leqslant \tau \leqslant 5125$, respectively. It is seen that β is close to $+135^\circ$ or -45° in Fig. 5(a). This means that the nodal diameter maintains its orientation and does not rotate. On the other hand, Figs. 5(b) and (c) reveal that β continuously varies with time. This means that the nodal diameter rotates counterclockwise then clockwise then counterclockwise and so on in an irregular manner.

Fig. 6 shows the response curves for the mean square response, $E[z_0^2]$, of the structure and the liquid mean square responses, $E[c_{11}^2]$ and $E[d_{11}^2]$, of the sloshing mode (1,1). The symbols • and ○ represent the numerical results, which are calculated by Monte Carlo simulations using 100 different sets of random number series, while the dash–dotted curve represents the theoretical result obtained from Eq. (24). In Fig. 6 and subsequent figures, the statistics are estimated from 100 different sets of time histories for duration of $t = 1000$ to 6000 of the time histories in order to

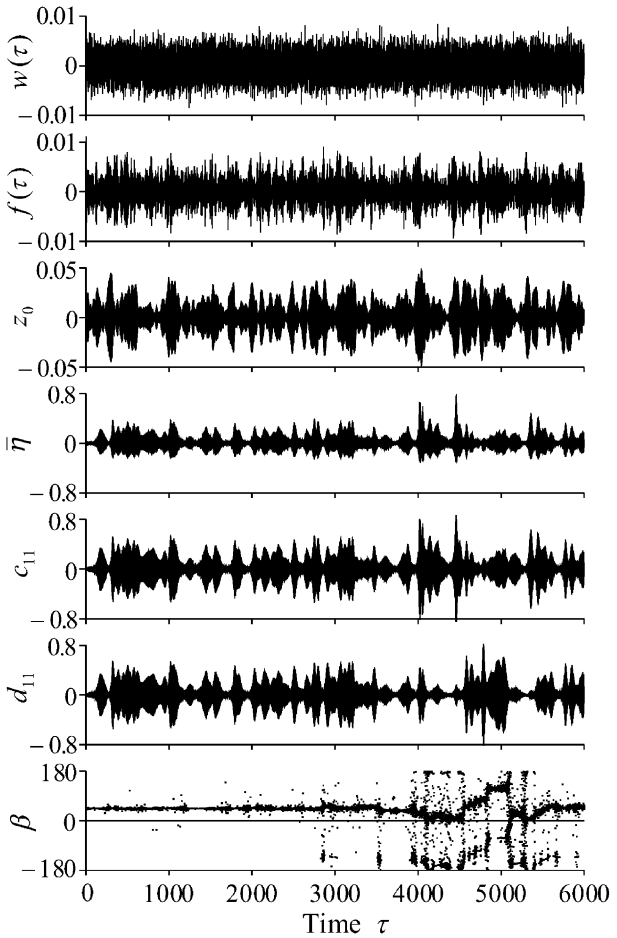

Fig. 3. Time histories in the coupled system when $\bar{h} = 1.2$, $\mu_1 = 0.87$, $\mu_2 = 0.034$, $\bar{k} = 4.0$, $\zeta = 0.03$, $\zeta_{01} = \zeta_{11} = \zeta_{21} = 0.01$, $S_0 = 2.0 \times 10^{-7}$, $\gamma = 0.1$, $\Omega = 2.0$ and $(\bar{r}, \theta) = (1, 0)$.

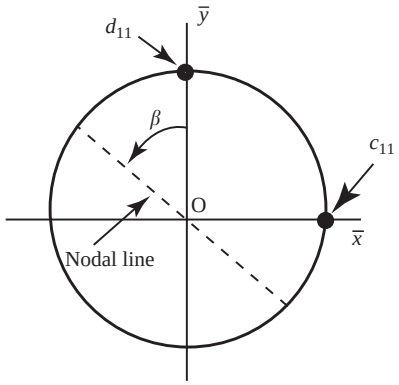

Fig. 4. The definition of the angular position β of the nodal diameter.

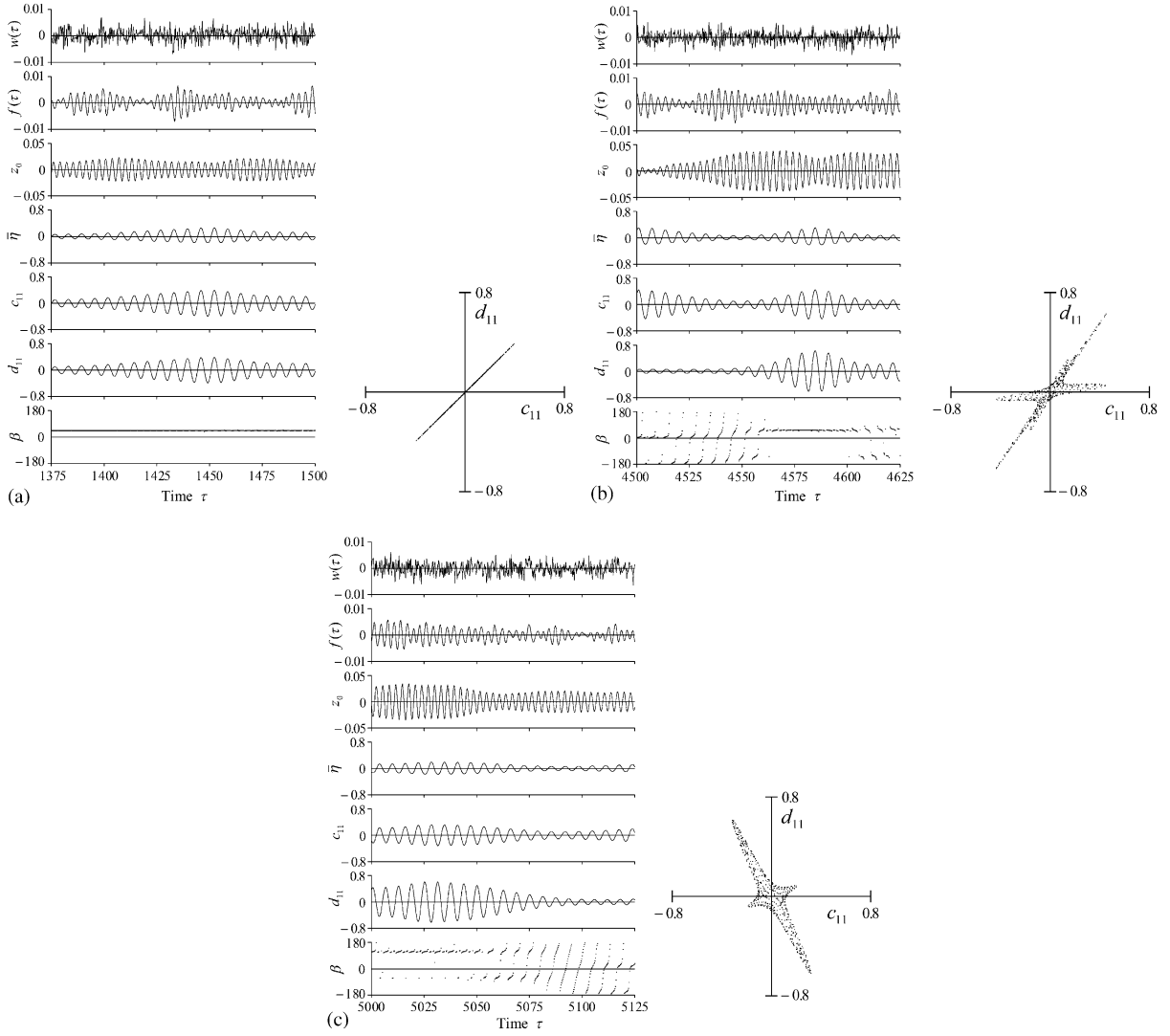

Fig. 5. Time histories magnified at each time interval in Fig. 3 and its trajectory on the (c_{11}, d_{11})-plane. (a) $1375 \leqslant \tau \leqslant 1500$. (b) $4500 \leqslant \tau \leqslant 4625$. (c) $5000 \leqslant \tau \leqslant 5125$.

eliminate the transient responses. Figs. 6(a)–(c) show the dependence of the mean square responses on the center frequency Ω of a narrow-band random excitation for three different values of bandwidth $\gamma = 0.1, 0.2$ and 0.3, respectively, and for the same parameters of Fig. 3. Comparing these results with those of the uncoupled system reveals that the mean square response, $E[z_0^2]$, in the coupled system drops over a finite range of Ω, where the liquid free surface motion interacts with the structure through nonlinear coupling. As the filter bandwidth, γ, increases, the peak of $E[z_0^2]$, shown by solid dots •, decreases, associated with a shrinking in the range of Ω, over which the interaction with liquid motion takes place.

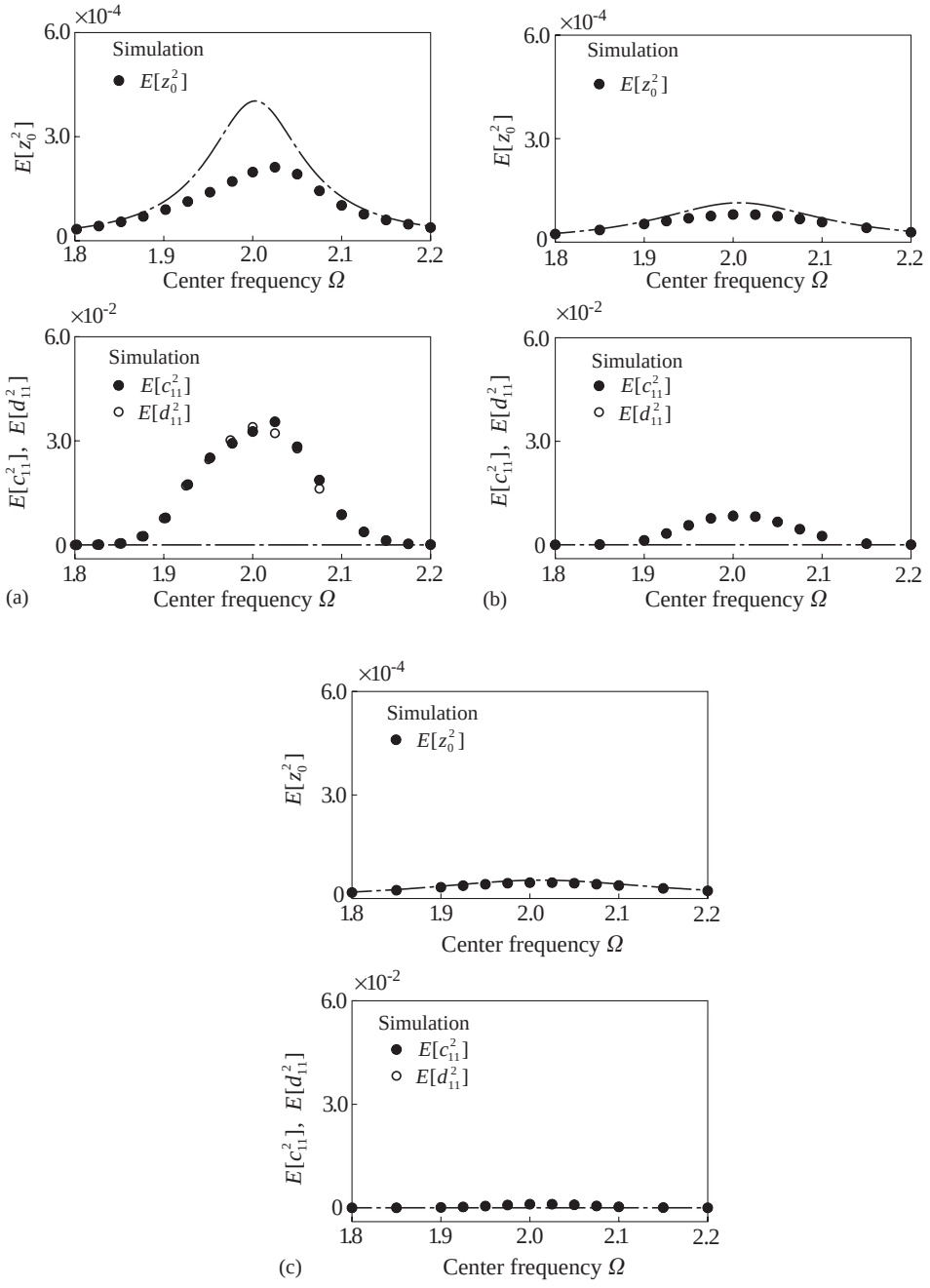

Fig. 6. Mean square response $E[z_0^2]$ for the structure displacement and mean square responses $E[c_{11}^2]$ and $E[d_{11}^2]$ for the liquid elevation, showing the influence of the center frequency Ω and the bandwidth γ, when the values of the other parameters are the same as those in Fig. 3. (a) $\gamma = 0.1$. (b) $\gamma = 0.2$. (c) $\gamma = 0.3$.

Fig. 7 shows the dependence of the normalized mean square of the structure $E[z_0^2]_c/E[z_0^2]_f$ on the center frequency for various values of bandwidth γ, where the subscript "c" denotes coupling, and "f" denotes frozen. This normalized representation provides direct information regarding the degree of nonlinear coupling and the energy transfer between the structure and liquid surface motions. It can be seen that the amount of the energy transfer from the structure motion to the liquid surface motion becomes predominant as γ decreases.

Fig. 8 shows the plots of the probability density function (pdf) of the structure displacement z_0 and liquid elevation $\bar{\eta}$ for (a) $\Omega = 1.9$, (b) $\Omega = 1.95$ and (c) $\Omega = 2.0$ according to Fig. 6(a). The dotted pdf plots represent the estimated results from simulation, and the solid curves represent the Gaussian pdf calculated from the mean and mean square values of z_0 and $\bar{\eta}$. The distribution $p(z_0)$ is almost Gaussian, while $p(\bar{\eta})$ is deviated from normality. Since the liquid elevation $\bar{\eta}$ exhibits zero-amplitude intervals in the time domain, $p(\bar{\eta})$ deviates from a Gaussian distribution when the center frequency is closer to the stability boundaries as will be demonstrated in Fig. 14. It should be noted that the response pdf curves of both structure and free surface height shown by solid curves exhibit asymmetry for $\Omega = 2.0$.

Fig. 9 shows the probability density functions $p(\mathrm{Amp}[z_0])$ and $p(\mathrm{Amp}[c_{11}])$ of the amplitudes of z_0 and c_{11} for (a) $\Omega = 1.9$, (b) $\Omega = 1.95$ and (c) $\Omega = 2.0$ in Fig. 6(a). These amplitudes are calculated using the following expressions:

$$\mathrm{Amp}[z_0] = \sqrt{z_0^2 + \dot{z}_0^2} \quad \text{and} \quad \mathrm{Amp}[c_{11}] = \sqrt{c_{11}^2 + \left(\frac{\dot{c}_{11}}{\Omega/2}\right)^2}. \tag{26}$$

The solid curves represent Rayleigh's distribution. It is obvious that the distribution $p(\mathrm{Amp}[z_0])$ coincides with a Rayleigh distribution, since z_0 exhibits a Gaussian process. $p(\mathrm{Amp}[c_{11}])$, however, deviates greatly from the Rayleigh distribution, especially for $\Omega = 1.9$, because its time history involves a lot of time intervals of zero amplitude.

Fig. 10 shows the dependence of the mean square response of the liquid amplitudes c_{11} and d_{11} on the excitation spectral density S_0. This figure is magnified in Fig. 11 and both figures reveal that the mean square value of the liquid elevation gradually increases as the intensity S_0 increases,

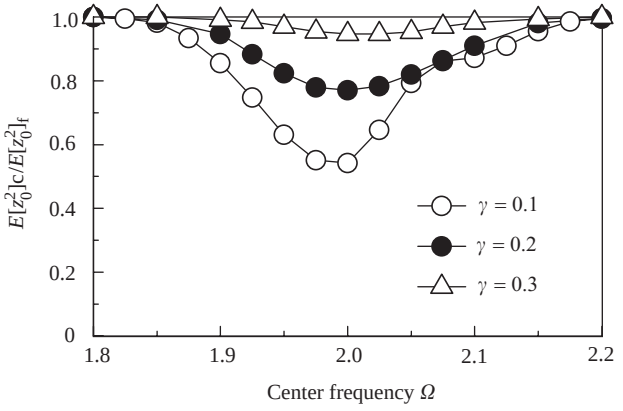

Fig. 7. Ratio of $E[z_0^2]_c$ in a coupled system to $E[z_0^2]_f$ in an uncoupled system for various values of bandwidth γ when $\bar{h} = 1.2$, $\mu_1 = 0.87$, $\mu_2 = 0.034$, $\bar{k} = 4.0$, $\zeta = 0.03$, $\zeta_{01} = \zeta_{11} = \zeta_{21} = 0.01$ and $\gamma = 0.1$.

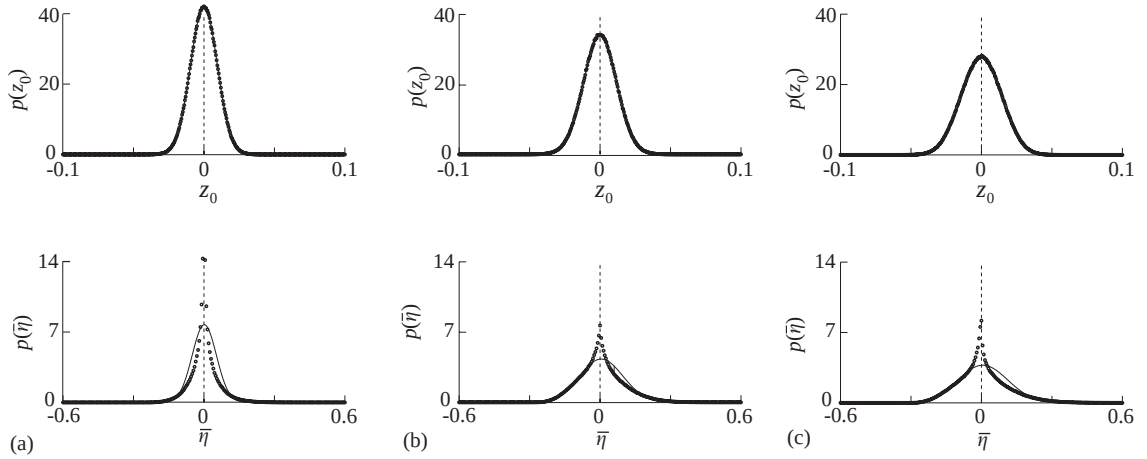

Fig. 8. Probability density distributions of the structure displacement z_0 and the liquid elevation $\bar{\eta}$ showing the influence of the center frequency Ω in Fig. 6(a).——, approximated Gaussian distribution; •, numerical simulation. (a) $\Omega = 1.9$, (b) $\Omega = 1.95$ and (c) $\Omega = 2.0$.

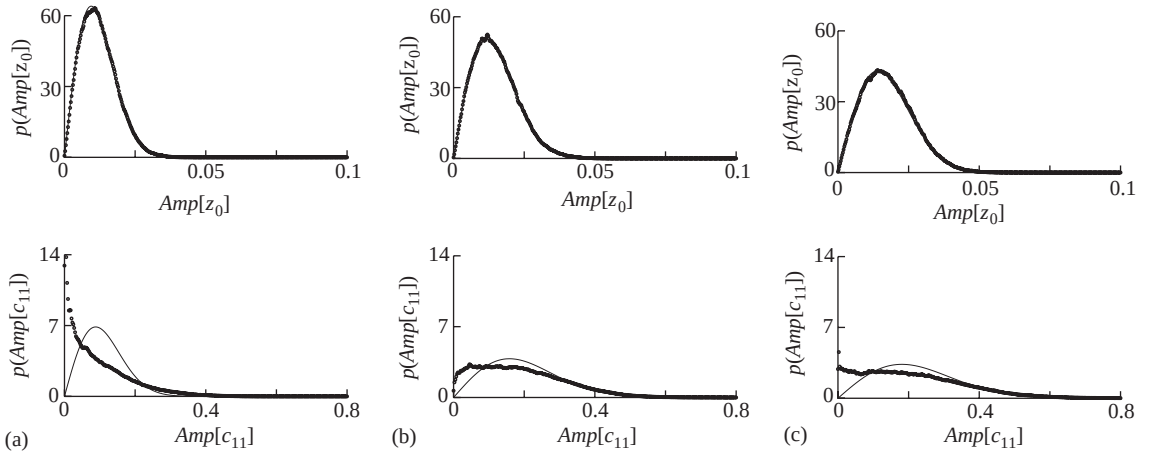

Fig. 9. Probability density distributions of the amplitudes of z_0 and c_{11} for different values of the center frequency Ω in Fig. 6(a). ——, approximated Rayleigh distribution; •, numerical simulation. (a) $\Omega = 1.9$, (b) $\Omega = 1.95$ and (c) $\Omega = 2.0$.

and that $E[c_{11}^2]$ is nearly equal to $E[d_{11}^2]$. The stability boundary of liquid sloshing is defined in this analysis by taking the value of the mean square level $A_{\mathrm{ms}} = 2.0 \times 10^{-4}$ that corresponds to $S_0 \approx 0.15 \times 10^{-7}$. This threshold mean square level refers either to mode c_{11} or mode d_{11}.

Fig. 12 shows the averaged time lengths of different regimes of liquid motion taken from 100 time history records for the same values of parameters as those in Fig. 10. These time history records reflect the way in which the energy is redistributed among the fluid and structure modes due to the presence of internal resonance and excitation level in addition to the physical properties of the system. The value $A_{\mathrm{ms}} = 2.0 \times 10^{-4}$ was defined in Fig. 11. This value corresponds to the

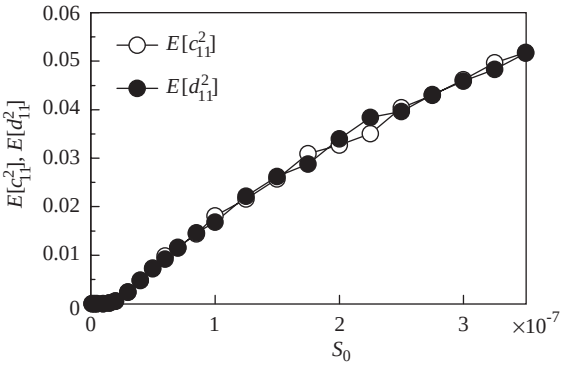

Fig. 10. Mean square values of c_{11} and d_{11} showing the influence of the excitation intensity S_0 when $\bar{h} = 1.2$, $\mu_1 = 0.87$, $\mu_2 = 0.034$, $\bar{k} = 4.0$, $\zeta = 0.03$, $\zeta_{01} = \zeta_{11} = \zeta_{21} = 0.01$, $\gamma = 0.1$ and $\Omega = 2.0$, i.e., these values except for S_0 are the same as in Fig. 3.

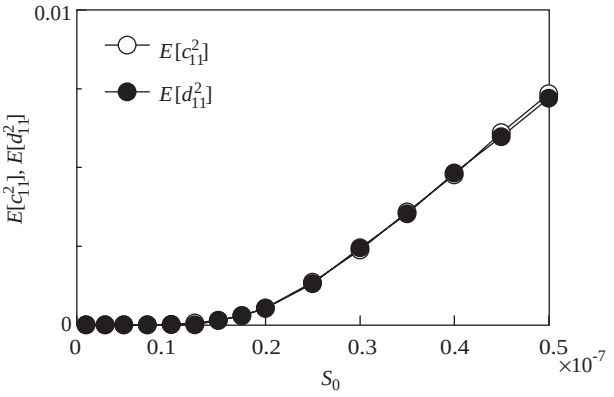

Fig. 11. Magnified graph of Fig. 10.

value $A_0 = 0.02$ of the amplitude of c_{11} or d_{11}, since the relation $A_0 = \sqrt{2A_{\text{ms}}}$ is satisfied. The time length T_{high} of high liquid level is defined when the amplitudes of c_{11} or d_{11} exceed the value A_0. From Figs. 11 and 12, four kinds of regions are identified depending on S_0 as reported in Ref. [29]. Region I corresponding to $S_0 \leqslant 0.15 \times 10^{-7}$ (zero liquid motion), where the liquid free surface is stable. Region II corresponding to $0.15 \times 10^{-7} \leqslant S_0 \leqslant 0.3 \times 10^{-7}$ (uncertain zero motion, or on-off intermittency), where the mean square values of c_{11} and d_{11} are very small, that is, T_{high} is close to zero, but the liquid sloshing occurs intermittently. In region II, T_{high} is less than 50% of whole time interval as shown in Fig. 12. Region III, $0.3 \times 10^{-7} \leqslant S_0 \leqslant 1.0 \times 10^{-7}$, corresponds to partially developed motion, i.e., large amplitude of sloshing occurs over a finite time interval and then decays for next time interval. Region IV, $S_0 \geqslant 1.0 \times 10^{-7}$, corresponding to fully developed motion and is characterized by continuous random liquid motion. In region IV the time length of high liquid level is more than 90% as shown in Fig. 12.

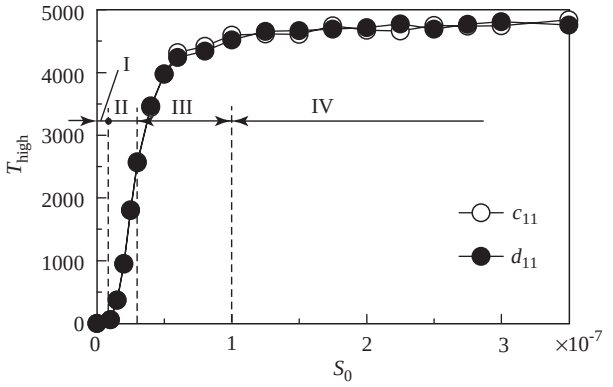

Fig. 12. Averaged time length of the high liquid level for the same values of parameters as those in Fig. 10. Region I: zero liquid motion; region II: uncertain zero motion; region III: partially developed motion; and region IV: fully developed motion.

Fig. 13 shows time history records for different excitation levels: (a) $S_0 = 0.25 \times 10^{-7}$, (b) $S_0 = 0.5 \times 10^{-7}$, (c) $S_0 = 1.5 \times 10^{-7}$ and (d) $S_0 = 3.5 \times 10^{-7}$. Figs. 13(a)–(d) correspond to regions II, III, IV, and IV, respectively. It is seen that the angular position β remains constant in region II of Fig. 13(a) and region III of Fig. 13(b). In region IV shown in Figs. 13(c) and (d), however, β changes during a part of time interval, and then β violently changes as S_0 increases much more as seen in Fig. 13(d).

Fig. 14 shows the stability boundaries in the parameter space (Ω, S_0) for $\gamma = 0.1$, 0.2 and 0.3, based on the definition of Fig. 12, i.e., the boundary between regions I and II. The values of the system parameters are the same as those in Fig. 3 except those values of Ω and S_0. The symbols •, ■ and ▲ stand for the unstable case where the liquid sloshing occurs, while ○, △ and □ represent the stable case where the liquid motion does not occur. It is seen that the unstable region becomes wider as γ decreases or as S_0 increases.

Fig. 15 shows the correlation coefficient between c_{11} and d_{11} calculated by the expression

$$\rho[c_{11}, d_{11}] = \frac{\sum_i (c_{11i} - E[c_{11}])(d_{11i} - E[d_{11}])}{\sqrt{\sum_i (c_{11i} - E[c_{11}])^2 \sum_i (d_{11i} - E[d_{11}])^2}}. \tag{27}$$

The function $\rho[c_{11}, d_{11}]$ gives the correlation between c_{11} and d_{11}. The shape of the time history of c_{11} is very similar to that of d_{11} when S_0 is small as shown in Figs. 13(a) and (b). For small S_0, both c_{11} and d_{11} are only excited independently and the intensity of interaction between them is very weak. In contrast, $\rho[c_{11}, d_{11}]$ is small when S_0 is comparatively large. In this case, the shape of time history of c_{11} becomes different from that of d_{11}, as shown in Figs. 3 and 13(d). This implies that the energy can be exchanged between c_{11} and d_{11}, due to the nonlinear coupling of the two modes.

Figs. 16(a) and (b) show the mean square responses when the liquid level is lower than that of Fig. 6(a). The values of parameters which differ from those in Fig. 6(a) are $\bar{h} = 0.55$, $\mu_1 = 0.94$ and $\mu_2 = 0.035$ in Fig. 16(a), while they are $\bar{h} = 0.40$, $\mu_1 = 0.96$ and $\mu_2 = 0.032$ in Fig. 16(b). As the

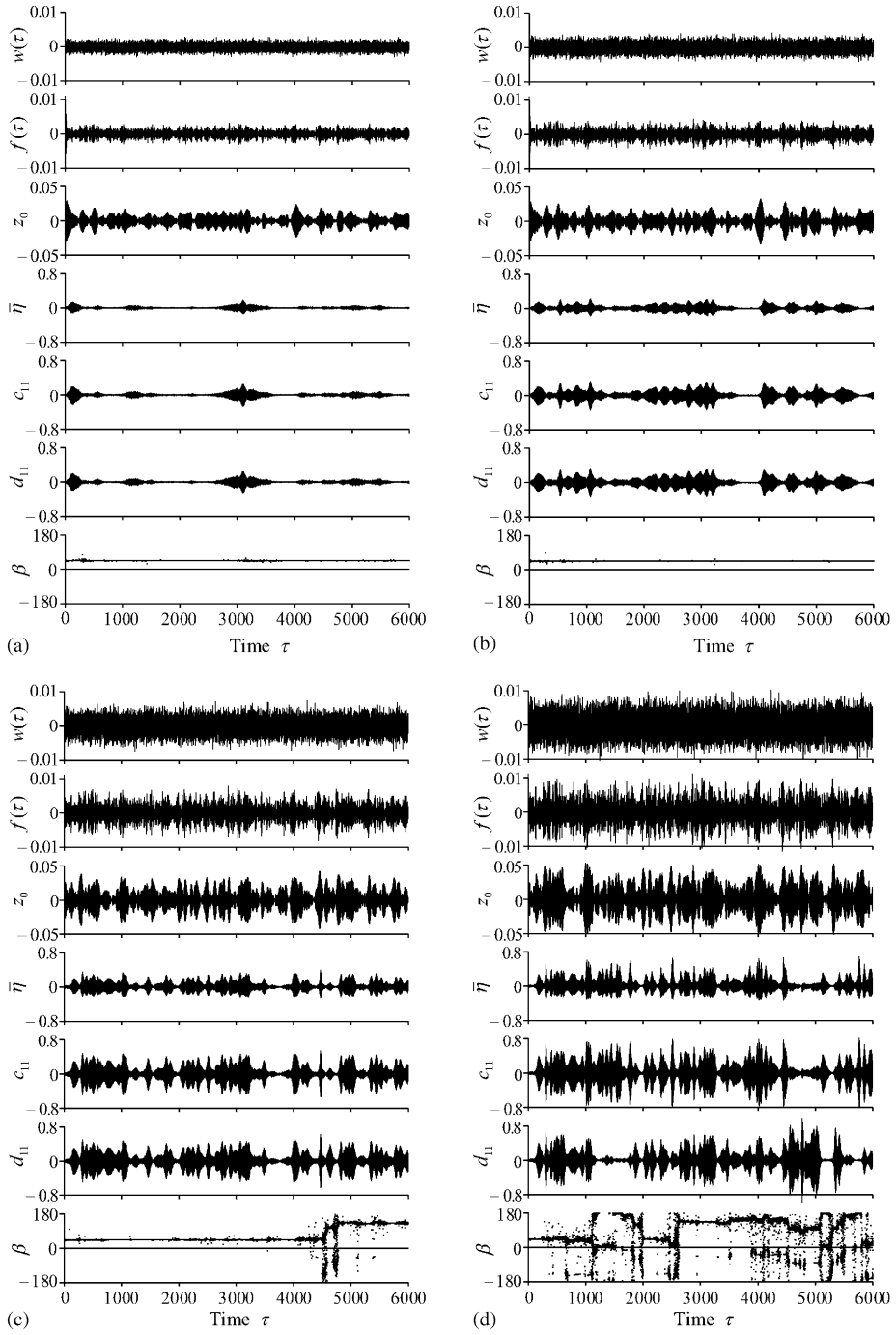

Fig. 13. Time histories showing the effects of excitation intensity for (a) $S_0 = 0.25 \times 10^{-7}$ (in region II), (b) $S_0 = 0.5 \times 10^{-7}$ (in region III), (c) $S_0 = 1.5 \times 10^{-7}$ (in region IV) and (d) $S_0 = 3.5 \times 10^{-7}$ (in region IV).

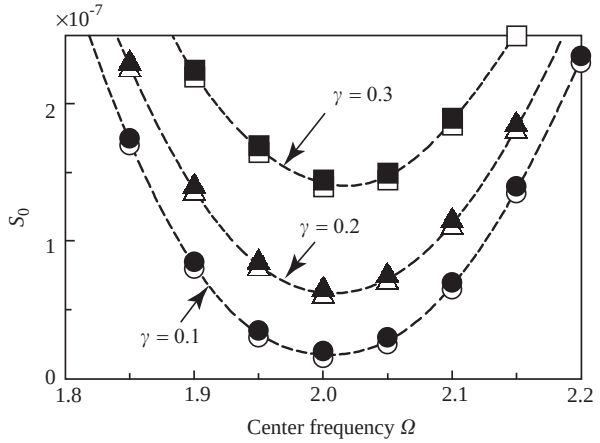

Fig. 14. The stability boundaries in a parameter space (Ω, S_0) for $\gamma = 0.1$, 0.2 and 0.3.

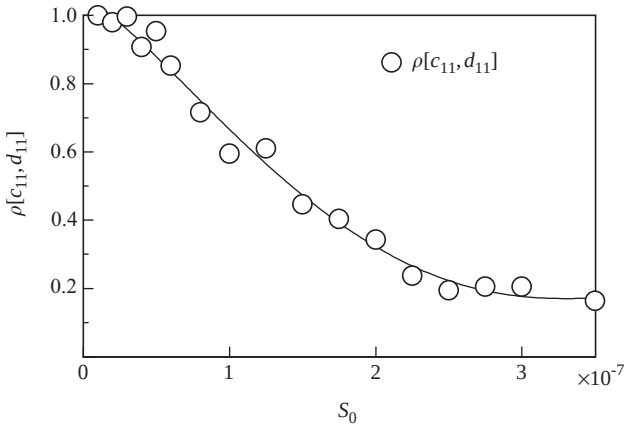

Fig. 15. Correlation coefficient between c_{11} and d_{11} showing the influence of the excitation intensity S_0 when $\bar{h} = 1.2$, $\mu_1 = 0.87$, $\mu_2 = 0.034$, $\bar{k} = 4.0$, $\zeta = 0.03$, $\zeta_{01} = \zeta_{11} = \zeta_{21} = 0.01$, $\gamma = 0.1$ and $\Omega = 2.0$.

value of $\bar{h}$ decreases, the range of Ω, where coupled vibrations occur shrinks and the mean square values $E[c_{11}^2]$ and $E[d_{11}^2]$ of liquid elevation decrease. In addition, as $\bar{h}$ decreases, the peak of the response $E[z_0^2]$ moves toward the left-hand side. This seems to come from the system characteristics associated with the frequency response curve in the case of a harmonic excitation [17].

Figs. 17(a) and (b) show the mean square responses for two different values of the spring constant $\bar{k} = 3.80$ and 3.67, respectively. By introducing the detuning parameter $\sigma_{11} = \bar{\omega}_s - 2\bar{\omega}_{11}$, Fig. 17(a) is obtained for $\sigma_{11} = -0.0489$, ($\bar{\omega}_s = 1.9511$, $\bar{\omega}_{11} = 1.0$), while Fig. 17(b) is for $\sigma_{11} = -0.0825$ ($\bar{\omega}_s = 1.9175$ and $\bar{\omega}_{11} = 1.0$). It is found that the peaks of the mean square responses

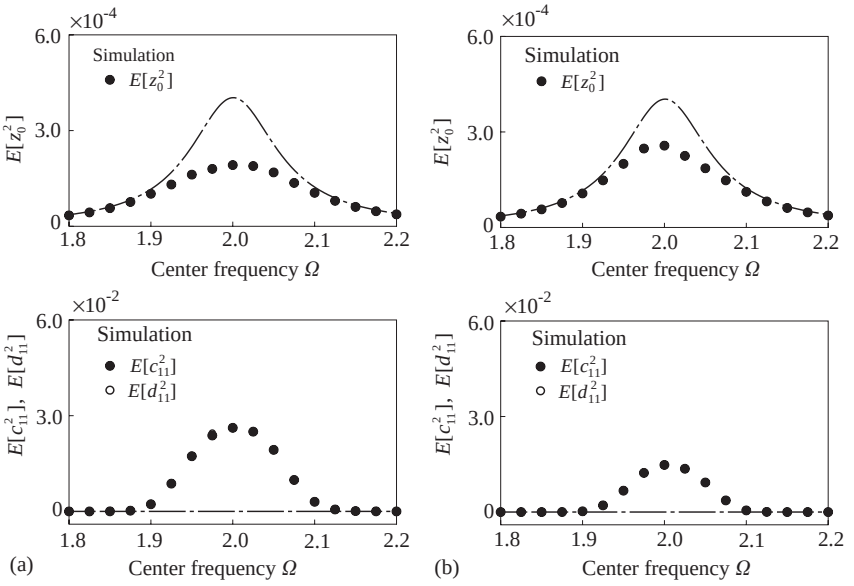

Fig. 16. Mean square responses as in Fig. 6(a) but for different values of $\bar{h}$. (a) $\bar{h} = 0.55$, $\mu_1 = 0.94$, $\mu_2 = 0.035$. (b) $\bar{h} = 0.40$, $\mu_1 = 0.96$, $\mu_2 = 0.032$.

$E[c_{11}^2]$ and $E[d_{11}^2]$ of liquid elevation in Figs. 17(a) are larger than those in Fig. 6(a), and that they become smaller than those in Fig. 6(a) as the absolute value of σ_{11} increases. In addition, as $\bar{k}$ decreases, the peak of the response $E[z_0^2]$ moves toward the left-hand side, like as shown in Fig. 16.

3.2. Uni-modal sloshing

The results of Section 3.1 considered the interaction with three sloshing modes (1,1), (0,1) and (2,1). It is useful to consider the simpler case of a single sloshing mode interacting with the structure in order to evaluate the structure's statistics. We set $d_{11} = c_{01} = d_{01} = c_{21} = d_{21} = 0$ in Eqs. (20). In this case, the structure displacement z_0 and the amplitude c_{11} are coupled. Fig. 18 shows the mean square responses of $E[z_0^2]$ and $E[c_{11}^2]$. It should be noted that the scale of the ordinate $E[c_{11}^2]$ in Fig. 18 is twice as large as that in Fig. 6(a), albeit the magnitude of $E[z_0^2]$ is almost the same as that in Fig. 6(a), while the magnitude of $E[c_{11}^2]$ in Fig. 18 is just twice the magnitude of that in Fig. 6(a). This may be attributed to the fact that the orthogonal mode is not coupled with the mode c_{11}. Thus, it is found that one can obtain the adequate results from the statistics of the structure response.

4. Conclusions

The random excitation of an elastic structure carrying a cylindrical liquid tank has been studied numerically in the neighborhood of 2:1 internal resonance. The analytical model was developed to

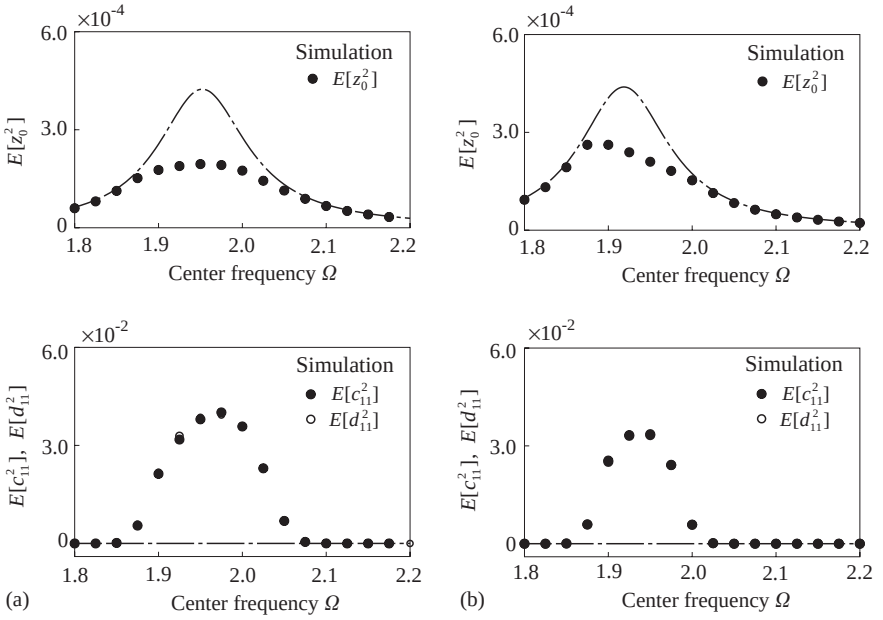

Fig. 17. Mean square responses as in Fig. 6(a) but for different values of $\bar{k}$. (a) $\bar{k} = 3.80$. (b) $\bar{k} = 3.67$.

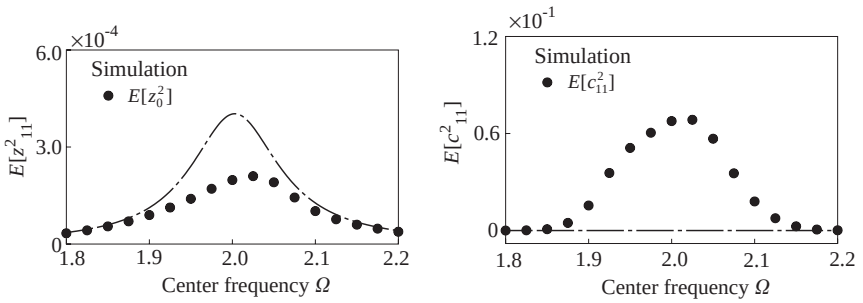

Fig. 18. Mean square responses for the uni-modal sloshing when the values of parameters are the same as in Fig. 6(a).

include three sloshing modes. It is found that over a narrow band of the excitation center frequency the liquid motion acts as a nonlinear vibration absorber of the structure response. The rotational (swirl) motion of liquid surface was found to occur more violently as the excitation intensity increases. The structure displacement response displayed a Gaussian process, while the liquid motion pdf deviated from a Gaussian distribution. The time history records generated for different excitation levels revealed four regimes of liquid surface motion: zero motion, uncertain motion, partially developed motion and fully developed motion. The unstable region, where the liquid sloshing occurs, becomes wider as the excitation intensity increases or when its bandwidth is reduced. A uni-modal sloshing modeling proved to be adequate to study the structure dynamic interaction with the liquid.

Acknowledgements

This paper was partially supported by grant-in-aid for Scientific Research from the Japanese Ministry of Education, Culture, Sports, Science and Technology. The first author would like to express his appreciation for their generous support.

Appendix A

Applying Newton's second law to a fluid particle in a nonviscous fluid, we can obtain the equations of motion in the moving coordinate system O–xyz or O–$r\theta z$ (see Fig. 1) as follows:

$$\rho \frac{\mathrm{d}\mathbf{v}}{\mathrm{d}t} = -\mathrm{grad}\, P + \rho\mathbf{g}, \tag{A.1}$$

where $\mathbf{v}$ is the velocity vector of the fluid particle which exists at the spatial position (x, y, z) at time t, and $\mathbf{g}$ is the vector of gravitational acceleration. By noting the fact that

$$\frac{\mathrm{d}\mathbf{v}}{\mathrm{d}t} = \frac{\partial \mathbf{v}}{\partial t} + (\mathbf{v}\cdot\mathrm{grad})\mathbf{v} \tag{A.2}$$

and taking into account $\mathrm{rot}\,\mathbf{v} = 0$ for an irrotational fluid, and using the equation

$$\frac{1}{2}\,\mathrm{grad}\, q^2 = \mathbf{v}\times\mathrm{rot}\,\mathbf{v} + (\mathbf{v}\cdot\mathrm{grad})\mathbf{v} = (\mathbf{v}\cdot\mathrm{grad})\mathbf{v}, \tag{A.3}$$

Eq. (A.1) may be rewritten

$$\frac{\partial \mathbf{v}}{\partial t} + \frac{1}{2}\,\mathrm{grad}\, q^2 = -\frac{\mathrm{grad}\, P}{\rho} + \mathbf{g}, \tag{A.4}$$

where $q = |\mathbf{v}|$. It should be noted that the velocity potential $\tilde{\Phi}$ can exist under the assumption of irrotational flow. Therefore the fluid velocity can be expressed by using $\tilde{\Phi}$ as follows:

$$\mathbf{v} = \mathrm{grad}\,\tilde{\Phi} (\equiv \nabla\tilde{\Phi}). \tag{A.5}$$

Substituting Eq. (A.5) into Eq. (A.4), we obtain

$$\mathrm{grad}\left(\frac{\partial\tilde{\Phi}}{\partial t}\right) + \frac{1}{2}\,\mathrm{grad}\, q^2 = -\frac{\mathrm{grad}\, P}{\rho} + \mathrm{grad}(-gz). \tag{A.6}$$

Therefore Eq. (A.6) may be rewritten

$$\mathrm{grad}\left(\frac{\partial\tilde{\Phi}}{\partial t} + \frac{1}{2}\,q^2 + \frac{P}{\rho} + gz\right) = 0. \tag{A.7}$$

Integrating Eq. (A.7), we obtain

$$\frac{\partial\tilde{\Phi}}{\partial t} + \frac{1}{2}\,q^2 + \frac{P}{\rho} + gz = c_1(t). \tag{A.8}$$

It is convenient to write the velocity potential $\tilde{\Phi}$ as the sum of the part corresponding to the tank motion, Φ_0, and the part corresponding to the fluid motion relative to the

tank, Φ, i.e.,

$$\tilde{\Phi} = \Phi_0 + \Phi. \tag{A.9}$$

The velocity of the tank $\mathbf{v}_0$ can be expressed by using Φ_0 and unit vectors $\mathbf{e}_r$, $\mathbf{e}_\theta$ and $\mathbf{e}_z$ in the cylindrical coordinate system as

$$\mathbf{v}_0 = \text{grad}\,\Phi_0 = \frac{\partial \Phi_0}{\partial r}\,\mathbf{e}_r + \frac{1}{r}\frac{\partial \Phi_0}{\partial \theta}\,\mathbf{e}_\theta + \frac{\partial \Phi_0}{\partial z}\,\mathbf{e}_z. \tag{A.10}$$

The velocity $\mathbf{v}_0$, i.e., the relative velocity of the origin O in the coordinate system O–xyz with respect to the fixed coordinate system O′–XYZ, can be also expressed by

$$\mathbf{v}_0 = \dot{Z}_0 \mathbf{e}_z, \tag{A.11}$$

where $\dot{Z}_0$ is the tank velocity since the tank is excited only in the vertical direction. Eqs. (A.10) and (A.11) lead to

$$\frac{\partial \Phi_0}{\partial r} = 0, \quad \frac{1}{r}\frac{\partial \Phi_0}{\partial \theta} = 0, \quad \frac{\partial \Phi_0}{\partial z} = \dot{Z}_0. \tag{A.12}$$

Integrating Eq. (A.12), we obtain

$$\Phi_0 = \dot{Z}_0 z + c_2(t). \tag{A.13}$$

Partial differentiation of Eq. (A.13) with respect of t yields

$$\frac{\partial \Phi_0}{\partial t} = \ddot{Z}_0 z + \dot{c}_2(t). \tag{A.14}$$

Substituting Eqs. (A.9) and (A.15) into Eq. (A.8), we obtain

$$\frac{\partial \Phi}{\partial t} + \ddot{Z}_0 z + \dot{c}_2(t) + \frac{1}{2}q^2 + \frac{P}{\rho} + gz = c_1(t). \tag{A.15}$$

If the velocity potential Φ is replaced by $\Phi + \int\{c_1(t) - \dot{c}_2(t)\}\,\mathrm{d}t$ in Eq. (A.15),

$$\frac{\partial \Phi}{\partial t} + \frac{1}{2}q^2 + \frac{P}{\rho} + gz = -\ddot{Z}_0 z. \tag{A.16}$$

Using the velocity potential Φ instead of the velocity q, Eq. (A.16) may be rewritten as

$$\frac{\partial \Phi}{\partial t} + \frac{1}{2}\left\{\left(\frac{\partial \Phi}{\partial r}\right)^2 + \frac{1}{r^2}\left(\frac{\partial \Phi}{\partial \theta}\right)^2 + \left(\frac{\partial \phi}{\partial z}\right)^2\right\} + \frac{P}{\rho} + gz = -\ddot{Z}_0 z. \tag{A.17}$$

Appendix B

The nonlinear terms G_i ($i = 1, 2, \ldots, 13$) in Eqs. (18) and (19) are expressed by

$$G_1 = Q_3(a_{11}^2 + b_{11}^2),$$

$$G_2 = Q_4\dot{a}_{01}c_{11} + Q_5\dot{a}_{11}c_{01} + Q_6\dot{a}_{11}c_{21} + Q_7\dot{a}_{21}c_{11} + Q_8\dot{b}_{11}d_{21} + Q_9\dot{b}_{21}d_{11} + Q_{10}(3\dot{a}_{11}c_{11}^2 + \dot{a}_{11}d_{11}^2 + 2\dot{b}_{11}c_{11}d_{11}) + Q_{11}a_{01}a_{11} + Q_{12}(a_{11}a_{21} + b_{11}b_{21}) + Q_{13}a_{11}^2c_{11} + Q_{14}b_{11}^2c_{11} + Q_{15}a_{11}b_{11}d_{11},$$

$$G_3 = Q_{16}\dot{a}_{01}d_{11} + Q_{17}\dot{b}_{11}c_{01} + Q_{18}\dot{a}_{11}d_{21} + Q_{19}\dot{a}_{21}d_{11} + Q_{20}\dot{b}_{11}c_{21} + Q_{21}\dot{b}_{21}c_{11} + Q_{22}(2\dot{a}_{11}c_{11}d_{11} + \dot{b}_{11}c_{11}^2 + 3\dot{b}_{11}d_{11}^2) + Q_{23}a_{01}b_{11} + Q_{24}(a_{11}b_{21} - a_{21}b_{11}) + Q_{25}a_{11}b_{11}c_{11} + Q_{26}a_{11}^2d_{11} + Q_{27}b_{11}^2d_{11},$$

$$G_4 = Q_{28}a_{01}c_{11} + Q_{29}a_{11}c_{01} + Q_{30}(a_{11}c_{21} + b_{11}d_{21}) + Q_{31}(a_{21}c_{11} + b_{21}d_{11}) + Q_{32}a_{11}c_{11}^2 + Q_{33}b_{11}c_{11}d_{11} + Q_{34}a_{11}d_{11}^2,$$

$$G_5 = Q_{35}a_{01}d_{11} + Q_{36}b_{11}c_{01} + Q_{37}(a_{11}d_{21} - b_{11}c_{21}) + Q_{38}(a_{21}d_{11} - b_{21}c_{11}) + Q_{39}b_{11}c_{11}^2 + Q_{40}a_{11}c_{11}d_{11} + Q_{41}b_{11}d_{11}^2,$$

$$G_6 = Q_{42}(\dot{a}_{11}c_{11} + \dot{b}_{11}d_{11}) + Q_{43}(a_{11}^2 + b_{11}^2), \quad G_7 = Q_{44}(\dot{a}_{11}c_{11} + \dot{b}_{11}d_{11}) + Q_{45}(a_{11}^2 + b_{11}^2),$$

$$G_8 = Q_{46}(a_{11}c_{11} + b_{11}d_{11}), \quad G_9 = Q_{47}(\dot{a}_{11}c_{11} - \dot{b}_{11}d_{11}) + Q_{48}(a_{11}^2 - b_{11}^2),$$
$$G_{10} = Q_{47}(\dot{a}_{11}d_{11} + \dot{b}_{11}c_{11}) + Q_{48}a_{11}b_{11}, \quad G_{11} = Q_{49}(a_{11}c_{11} - b_{11}d_{11}),$$
$$G_{12} = Q_{49}(a_{11}d_{11} + b_{11}c_{11}), \quad G_{13} = Q_{50}(\dot{a}_{11}c_{11} + \dot{b}_{11}d_{11}) + Q_{51}(a_{11}^2 + b_{11}^2), \tag{B.1}$$

where the coefficients Q_i $(i = 1, 2, \ldots, 51)$ are given by

$$Q_1 = \mu_1 + \pi\mu_2\bar{h}, \quad Q_2 = -\pi\mu_2, \quad Q_3 = -\frac{\pi\mu_2\alpha}{2\cosh^2(\xi_{11}\bar{h})}, \quad Q_4 = \psi_{01}K_1^{120},$$

$$Q_5 = \psi_{11}K_1^{120}, \quad Q_6 = \tfrac{1}{2}\psi_{11}K_1^{021}, \quad Q_7 = \tfrac{1}{2}\psi_{21}K_1^{021}, \quad Q_8 = Q_6, \quad Q_9 = Q_7,$$

$$Q_{10} = \tfrac{1}{8}\xi_{11}^2K_1^{040}, \quad Q_{11} = \gamma_1^{101} + \psi_{01}\psi_{11}K_1^{120}, \quad Q_{12} = \tfrac{1}{2}(\gamma_1^{112} + 2\kappa_1^{021} + \psi_{11}\psi_{21}K_1^{021}),$$

$$Q_{13} = \tfrac{1}{4}\psi_{11}(3\Gamma_1^{1111} + \kappa_1^{040} + 3\xi_{11}^2K_1^{040}), \quad Q_{14} = \tfrac{1}{4}\psi_{11}(\Gamma_1^{1111} + 3\kappa_1^{040} + \xi_{11}^2K_1^{040}),$$

$$Q_{15} = \tfrac{1}{2}\psi_{11}(\Gamma_1^{1111} - \kappa_1^{040} + \xi_{11}^2K_1^{040}), \quad Q_{16} = Q_4, \quad Q_{17} = Q_5, \quad Q_{18} = Q_6, \quad Q_{19} = -Q_7,$$

$$Q_{20} = -Q_8, \quad Q_{21} = Q_9, \quad Q_{22} = Q_{10}, \quad Q_{23} = Q_{11}, \quad Q_{24} = Q_{12}, \quad Q_{25} = Q_{15},$$

$$Q_{26} = Q_{14}, \quad Q_{27} = Q_{13}, \quad Q_{28} = \gamma_1^{101} - \xi_{01}^2K_1^{120}, \quad Q_{29} = \gamma_1^{101} - \xi_{11}^2K_1^{120},$$

$$Q_{30} = \tfrac{1}{2}(\gamma_1^{112} + 2\kappa_1^{021} - \xi_{11}^2K_1^{021}), \quad Q_{31} = \tfrac{1}{2}(\gamma_1^{112} + 2\kappa_1^{021} - \xi_{21}^2K_1^{021}),$$

$$Q_{32} = \tfrac{1}{8}\psi_{11}(6\Gamma_1^{1111} + 2\kappa_1^{040} - 3\xi_{11}^2K_1^{040}), \quad Q_{33} = \tfrac{1}{4}\psi_{11}(2\Gamma_1^{1111} + 2\kappa_1^{040} - \xi_{11}^2K_1^{040}),$$

$$Q_{34} = \tfrac{1}{8}\psi_{11}(2\Gamma_1^{1111} - 2\kappa_1^{040} - \xi_{11}^2 K_1^{040}), \quad Q_{35} = Q_{28}, \quad Q_{36} = Q_{29}, \quad Q_{37} = Q_{30},$$
$$Q_{38} = -Q_{31}, \quad Q_{39} = Q_{34}, \quad Q_{40} = Q_{33}, \quad Q_{41} = Q_{32}, \quad Q_{42} = \psi_{11} G_{11},$$
$$Q_{43} = \tfrac{1}{2}(\alpha + g_{11} + \psi_{11}^2 G_{11}), \quad Q_{44} = \tfrac{1}{2}\psi_{11} K_0^{120},$$
$$Q_{45} = \tfrac{1}{4}(\gamma_0^{011} + \kappa_0^{120} + \psi_{11}^2 K_0^{120}), \quad Q_{46} = \tfrac{1}{2}(\gamma_0^{011} + \kappa_0^{120} - \xi_{11}^2 K_0^{120}),$$
$$Q_{47} = \tfrac{1}{2}\psi_{11} K_2^{021}, \quad Q_{48} = \tfrac{1}{4}(\gamma_2^{211} - \kappa_2^{021} + \psi_{11}^2 K_2^{021}),$$
$$Q_{49} = \tfrac{1}{2}(\gamma_2^{211} - \kappa_2^{021} - \xi_{11}^2 K_2^{021}), \quad Q_{50} = -Q_2 Q_{42}, \quad Q_{51} = Q_3 - Q_2 Q_{43}. \tag{B.2}$$

The symbols in Eq. (B.2) are as follows:

$$G_{m1} = \int_0^1 \bar{r} \mathrm{J}_m^2(\xi_{m1}\bar{r})\,\mathrm{d}\bar{r}, \quad g_{m1} = \int_0^1 \frac{1}{\bar{r}} \mathrm{J}_m^2(\xi_{m1}\bar{r})\,\mathrm{d}\bar{r},$$
$$K_m^{ijk} = \int_0^1 \bar{r} \mathrm{J}_0^i(\xi_{01}\bar{r}) \mathrm{J}_1^j(\xi_{11}\bar{r}) \mathrm{J}_2^k(\xi_{21}\bar{r})\,\mathrm{d}\bar{r}/G_{m1},$$
$$\alpha = \int_0^1 \bar{r}\left\{\frac{\mathrm{d}\mathrm{J}_1(\xi_{11}\bar{r})}{\mathrm{d}\bar{r}}\right\}^2 \mathrm{d}\bar{r} = \frac{1}{4}\xi_{11}^2 \int_0^1 \bar{r}\{\mathrm{J}_0(\xi_{11}\bar{r}) - \mathrm{J}_2(\xi_{11}\bar{r})\}\,\mathrm{d}\bar{r},$$
$$\kappa_m^{ijk} = \int_0^1 \frac{1}{\bar{r}} \mathrm{J}_0^i(\xi_{01}\bar{r}) \mathrm{J}_1^j(\xi_{11}\bar{r}) \mathrm{J}_2^k(\xi_{21}\bar{r})\,\mathrm{d}\bar{r}/G_{m1},$$
$$\Gamma_m^{ijkl} = \int_0^1 \bar{r} \mathrm{J}_i(\xi_{i1}\bar{r}) \mathrm{J}_j(\xi_{j1}\bar{r}) \frac{\mathrm{d}}{\mathrm{d}\bar{r}}[\mathrm{J}_k(\xi_{k1}\bar{r})] \frac{\mathrm{d}}{\mathrm{d}\bar{r}}[\mathrm{J}_l(\xi_{l1}\bar{r})]\,\mathrm{d}\bar{r}/G_{m1},$$
$$\gamma_m^{ijk} = \int_0^1 \bar{r} \mathrm{J}_i(\xi_{i1}\bar{r}) \frac{\mathrm{d}}{\mathrm{d}\bar{r}}[\mathrm{J}_j(\xi_{j1}\bar{r})] \frac{\mathrm{d}}{\mathrm{d}\bar{r}}[\mathrm{J}_k(\xi_{k1}\bar{r})]\,\mathrm{d}\bar{r}/G_{m1},$$
$$\psi_{mn} = \xi_{mn}\tanh(\xi_{mn}\bar{h}). \tag{B.3}$$

The nonlinear terms H_l ($l = 1, 2, \ldots, 6$) in Eq. (20) are given by

$$H_1 = S_1(1 + \psi_{11}\ddot{z}_0)(c_{11}^2 + d_{11}^2) + S_2(\dot{c}_{11}^2 + \dot{d}_{11}^2),$$
$$H_2 = S_3\dot{c}_{01}\dot{c}_{11} + S_4(\dot{c}_{11}\dot{c}_{21} + \dot{d}_{11}\dot{d}_{21}) + S_5 c_{11}\dot{c}_{11}^2 + S_6 c_{11}\dot{d}_{11}^2 + S_7\dot{c}_{11}\dot{d}_{11}d_{11}$$
$$+ S_8 c_{01}c_{11} + S_9 c_{11}c_{21} + S_{10}d_{11}d_{21} + S_{11}c_{11}^3 + S_{12}c_{11}d_{11}^2,$$

$$H_3 = S_{13}\dot{c}_{01}\dot{d}_{11} + S_{14}(\dot{c}_{11}\dot{d}_{21} - \dot{c}_{21}\dot{d}_{11}) + S_{15}\dot{c}_{11}^2 d_{11} + S_{16}\dot{d}_{11}^2 d_{11} + S_{17}c_{11}\dot{c}_{11}\dot{d}_{11} + S_{18}c_{01}d_{11} + S_{19}c_{11}d_{21} + S_{20}c_{21}d_{11} + S_{21}d_{11}^3 + S_{22}c_{11}^2 d_{11},$$

$$H_4 = S_{23}(1 + \psi_{11}\ddot{z}_0)(c_{11}^2 + d_{11}^2) + S_{24}(\dot{c}_{11}^2 + \dot{d}_{11}^2),$$

$$H_5 = S_{25}(1 + \psi_{11}\ddot{z}_0)(c_{11}^2 - d_{11}^2) + S_{26}(\dot{c}_{11}^2 - \dot{d}_{11}^2),$$

$$H_6 = S_{27}(1 + \psi_{11}\ddot{z}_0)c_{11}d_{11} + S_{28}\dot{c}_{11}\dot{d}_{11}, \tag{B.4}$$

where S_i $(i = 1, 2, \ldots, 28)$ are constants determined by the system parameters.

References

[1] D.D. Kana, Interaction between liquid propellants and the elastic structure, in: H.N. Abramson (Ed.), *The Dynamic Behavior of Liquids in Moving Containers*, NASA SP-106, 1966, pp. 303–352 (Chapter 9).

[2] S.S. Chen, *Flow-Induced Vibration of Circular Cylindrical Tubes*, Hemisphere Publications, New York, 1987.

[3] M.P. Paidoussis, *Fluid–Structure Interactions*: *Slender Structures and Axial Flow*, Vol. 1, Academic Press, London, 1998.

[4] R.A. Ibrahim, V.N. Pilipchuk, T. Ikeda, Recent advances in liquid sloshing dynamics, *ASME Applied Mechanics Reviews* 54 (2) (2001) 133–199.

[5] M. Ifrim, C. Bratu, The effect of seismic action on the dynamic behavior of elevated water tanks, *Proceedings of the Fourth World Conference on Earthquake Engineering*, Vol. B-4, Santiago, 1969, pp. 127–142.

[6] Y. Sonobe, T. Nishikawa, Study of the earthquake proof design of elevated water tanks, *Proceedings of the Fourth World Conference on Earthquake Engineering*, Vol. B-4, Santiago, 1969, pp. 11–24.

[7] F.C. van Erp, Oscillation problems with a water tower, *Ingenieur* 81 (42) (1969) 148–152 (in German).

[8] R. Shepherd, The two mass representation of a water tower structure, *Journal of Sound and Vibration* 23 (3) (1969) 391–396.

[9] R.A. Ibrahim, A.D.S. Barr, Autoparametric resonance in a structure containing a liquid, Part I: two mode interaction, *Journal of Sound and Vibration* 42 (2) (1975) 159–179.

[10] R.A. Ibrahim, A.D.S. Barr, Autoparametric resonance in a structure containing a liquid, Part II: three mode interaction, *Journal of Sound and Vibration* 42 (2) (1975) 181–200.

[11] R.A. Ibrahim, Multiple internal resonance in a structure-liquid system, *Transactions of the ASME, Journal of Engineering for Industry* 98 (3) (1976) 1092–1098.

[12] R.A. Ibrahim, W. Li, Parametric and autoparametric vibrations of an elevated water tower, Part II: autoparametric response, *Journal of Sound and Vibration* 121 (3) (1988) 429–444.

[13] T. Ikeda, N. Nakagawa, Nonlinear vibrations of a structure caused by water sloshing in a rectangular tank, *Journal of Sound and Vibration* 201 (1) (1997) 23–41.

[14] T. Ikeda, T. Hirayama, N. Nakagawa, Nonlinear vibrations of a structure caused by water sloshing in a cylindrical tank, *JSME International Journal, Series C* 41 (3) (1998) 639–651.

[15] T. Ikeda, Nonlinear parametric vibrations of an elastic structure with a rectangular liquid tank, *Nonlinear Dynamics* 33 (1) (2003) 43–70.

[16] T. Ikeda, S. Murakami, Nonlinear vibrations of an elastic structure subjected to vertical excitation and coupled with liquid sloshing in a cylindrical tank (resonance with an axisymmetric mode), *Proceedings of the ASME 1999 Design Engineering Technical Conferences*, Las Vegas, NV, September 12–16 (1999), DETC99/VIB-8048.

[17] T. Ikeda, S. Murakami, Nonlinear parametric vibrations of an elastic structures subjected to vertical excitation and coupled with liquid sloshing in a cylindrical tank (resonance with an anti-symmetric mode), *Proceedings of the*

ASME 2001 Design Engineering Technical Conferences, Pittsburgh, PA, September 9–12, (2001), DETC2001/VIB-21650.

[18] O.S. Limarchenko, V.V. Yasinsky, *Nonlinear Dynamics of Constructions with a Fluid*, Kiev Polytechnic University, 1996 (in Russian).

[19] I.A. Lukovskii, A.N. Timokha, *Variational Methods in Nonlinear Dynamics of a Limited Liquid Volume*, Institute of Mathematics, Kiev, 1995 (in Russian).

[20] M.A. Haroun, H.M. Elliathy, Seismically induced fluid forces on elevated tanks, *ASCE Journal of Technical Topics in Civil Engineering* 111 (1985) 1–15.

[21] M.A. Haroun, H.M. Elliathy, Model for flexible tanks undergoing rocking, *ASCE Journal of Engineering Mechanics* 111 (2) (1985) 143–157.

[22] M.A. Haroun, L.R. Lee, H.M. Elliathy, Dynamic behavior of shell towers supporting liquid filled tanks, Sloshing and fluid structure vibration, *ASME Pressure Vess Piping Conference*, PVP–Vol 157, 1989, pp. 1–8.

[23] A. Kareem, W.-J. Sun, Stochastic response of structures with fluid-containing appendages, *Journal of Sound and Vibration* 119 (3) (1987) 398–408.

[24] A. Soundararajan, R.A. Ibrahim, Parametric and autoparametric vibrations of an elevated water tower, Part III: random response, *Journal of Sound and Vibration* 121 (3) (1988) 445–462.

[25] S. Kaneko, O. Yoshida, Modeling of deepwater-type rectangular tuned liquid damper with submerged nets, *Transactions of the ASME, Journal of Pressure Vessel Technology* 121 (4) (1999) 413–422.

[26] K. Yamamoto, M. Kawahara, Structural oscillation control using tuned liquid damper, *Computers and Structures* 71 (1999) 435–446.

[27] M. Sakata, K. Kimura, M. Utsumi, Non-stationary response of non-linear liquid motion in a cylindrical tank subjected to random base excitation, *Journal of Sound and Vibration* 94 (3) (1984) 351–363.

[28] G.E.P. Box, M.E. Muller, A note on the generation of random normal deviates, *Annals of Mathematics and Statistics* 28 (1958) 610–611.

[29] R.A. Ibrahim, R.T. Heinrich, Experimental investigation of liquid sloshing under parametric random excitation, *Transactions of the ASME, Journal of Applied Mechanics* 55 (2) (1988) 467–473.